

HERD: Continuous Human-to-Robot Evolution for Learning from Human Demonstration

Xingyu Liu Deepak Pathak Kris M. Kitani
Carnegie Mellon University

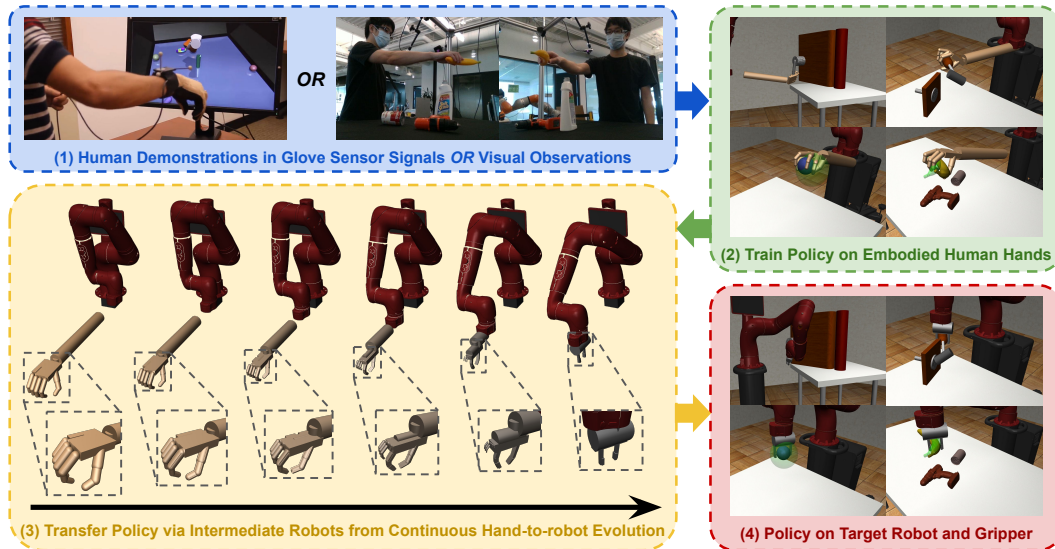


Figure 1: **HERD framework:** (1) Given human demonstrations in sensor glove signals [1] or visual data [2], (2) expert policies on an embodied human hand, i.e. a five-finger dexterous robot, can be trained. (3) We then design continuous robot evolution to connect the five-finger dexterous robot and a target commercial two-finger-gripper robot. A smooth curriculum of policy optimization on the intermediate robots that gradually evolves towards the target robot allows (4) the expert policies to be transferred to the target robot even in challenging sparse-reward tasks.

Abstract: The ability to learn from human demonstration endows robots with the ability to automate various tasks. However, directly learning from human demonstration is challenging since the structure of the human hand can be very different from the desired robot gripper. In this work, we show that manipulation skills can be transferred from a human to a robot through the use of micro-evolutionary reinforcement learning, where a five-finger human dexterous hand robot gradually evolves into a commercial robot, while repeatedly interacting in a physics simulator to continuously update the policy that is first learned from human demonstration. To deal with the high dimensions of robot parameters, we propose an algorithm for multi-dimensional evolution path searching that allows joint optimization of both the robot evolution path and the policy. Through experiments on human object manipulation datasets, we show that our framework can efficiently transfer the expert human agent policy trained from human demonstrations in diverse modalities to target commercial robots.

1 Introduction

Learning from human demonstrations [3] is a promising direction to enable robots to perform diverse manipulation capabilities. Recent large-scale visual datasets of human activity [2, 4, 5, 6, 7] have highlighted the need for enabling robotic agents to learn from human activities to perform diverse tasks in real-world environments. Existing paradigms for learning from human demonstration

generally follow the pipeline of *demonstration conversion*, i.e. (1) *convert demonstrated human states to robot states* and then (2) *train the robot policy*. Though step (2) can be solved by existing imitation learning approaches [8, 9, 10, 1], step (1) is extremely difficult. Efforts to address step (1) include human-robot observation matching such as [11], and converting human demonstrations to robots by human-robot interaction [12, 13] or human-in-the-loop teleoperation [14, 15]. However, these solutions are highly situational and task-specific and require significant human intervention for each individual task, therefore are not scalable and cannot automatically generalize to new tasks.

We propose a new paradigm for learning from human demonstration — *policy transformation*, i.e. (1) *train policy on embodied human hand dexterous robot* and then (2) *transfer the policy from dexterous hand robot to the target robot*. Many existing methods have been shown successful in learning control policy for dexterous hand robots from human demonstration [1, 16] and can easily solve step (1) of our pipeline. A general and automatic solution of step (2) would render a scalable solution of learning from human demonstration. The key challenge to step (2) is the huge dynamics discrepancy between the dexterous hand robot and the target robot. The discrepancy stems from the mismatch in robot morphology and kinematics. Unfortunately, statistical matching imitation learning approaches such as [8, 9, 10, 17] assume the teacher and student robotic agents share the same or similar transition dynamics, therefore are ineffective in solving the problem.

In this paper, we present a framework named *HERD* (short for *H*uman *E*volution to *R*obot for Learning from *D*emonstration) with a new perspective on solving the problem of learning from human demonstration — *continuous robot evolution*. Following the philosophy introduced in the seminal work of REvolveR [18], the core idea of our framework is to define a continuous interpolation between the dexterous hand robot and a target robot that have different morphology. Then an expert dexterous hand robot policy learned with methods such as [1, 16] can be transferred to the target robot through training on a sequence of intermediate robots that gradually evolve into the target robot. The policy is continuously updated through repeated interaction in a physics engine that contains the intermediate robots, as illustrated in Figure 1.

To instantiate the idea, we develop two solutions for the evolution from five-finger dexterous robot to two target commercial robots respectively: a Sawyer robot with a two-finger Rethink gripper, and a Jaco robot with a three-finger Jaco gripper. The solutions precisely match the dynamics of target commercial grippers. To deal with the high dimensions of robot parameters, we propose an algorithm for automatically searching evolution paths in high-dimensional robot parameter space that allows joint optimization of both robot evolution and the policy, based on online estimation of reward gradient with respect to robot evolution.

We conduct experiments on transferring human expert demonstrations of manipulation tasks in diverse modalities to the target commercial robots. We show that HERD can successfully transfer the expert dexterous hand robot policy trained from Hand Manipulation Suite sensor glove demonstrations [1] to the target robots even with sparse rewards. On DexYCB dataset [2], we demonstrate that our approach can also transfer the expert policy trained with visual human demonstrations to the target robots. In addition, we show that the proposed multi-dimensional robot evolution path search algorithm can significantly improve the policy transferring efficiency.

2 Preliminaries

MDP Preliminary We consider a continuous control problem formulated as Markov Decision Process (MDP). It is defined by a tuple $(\mathcal{S}, \mathcal{A}, \mathcal{T}, R, \gamma)$, where $\mathcal{S} \subseteq \mathbb{R}^S$ is the state space, $\mathcal{A} \subseteq \mathbb{R}^A$ is the action space, $\mathcal{T} : \mathcal{S} \times \mathcal{A} \rightarrow \mathcal{S}$ is the transition function, $R : \mathcal{S} \times \mathcal{A} \rightarrow \mathbb{R}$ is the reward function, and $\gamma \in [0, 1]$ is the discount factor. A policy $\pi : \mathcal{S} \rightarrow \mathcal{A}$ maps a state to an action where $\pi(a|s)$ is the probability of choosing action a at state s . Suppose \mathcal{M} is the set of all MDPs and $\rho^{\pi, M} = \sum_{t=0}^{\infty} \gamma^t R(s_t, a_t)$ is the episode discounted reward with policy π on MDP $M \in \mathcal{M}$. The optimal policy π_M^* on MDP M is the one that maximizes the expected value of $\rho^{\pi, M}$.

REvolveR [18] Preliminary Liu et al. [18] proposed a technique named REvolveR for transferring policies from a source robot to a target robot. The core idea is to define an evolutionary sequence of intermediate robots that connects the source to the target robot. Given source and target robots represented by two MDPs $M_S, M_T \in \mathcal{M}$ respectively, REvolveR defines a continuous function $E : [0, 1] \rightarrow \mathcal{M}$ where $E(0) = M_S, E(1) = M_T$. Then an expert policy $\pi_{E(0)}^*$ on the source robot $E(0)$ is optimized by sequentially interacting with each intermediate robot in the sequence

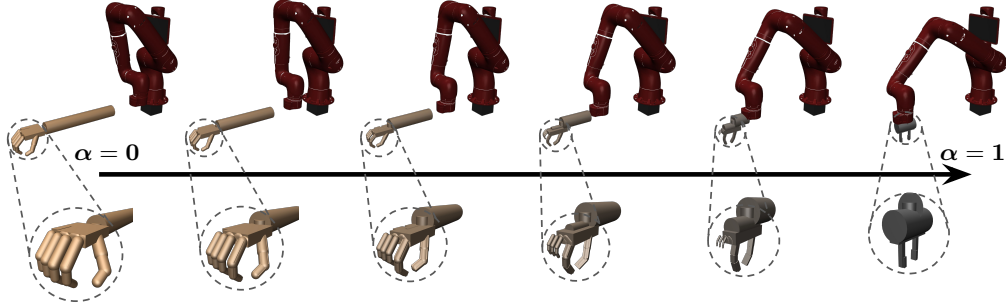


Figure 2: **Continuous hand-to-robot evolution for Sawyer robot.** We show one evolution path from human dexterous hand ($\alpha = 0$) to a commercial Sawyer robot with two-finger Rethink gripper ($\alpha = 1$). From left to right, we show intermediate robots along the path. Zoom in for better view.

$E(\alpha_1), E(\alpha_2), \dots, E(\alpha_K)$ where $0 < \alpha_1 < \alpha_2 < \dots < \alpha_K = 1$, until the policy is able to act (near) optimally on each intermediate robot and eventually transfer the policy to target robot $E(1)$. For all i , $|\alpha_{i+1} - \alpha_i|$ is small enough so that each policy fine-tuning step is a much easier task. Our method is built upon the philosophy of REvolveR to use robot evolution for policy transfer.

Notation We use bold letters to denote the vector variables. Specially, $\mathbf{0}$ and $\mathbf{1}$ are the all-zero and all-one vectors with proper dimensions respectively. $S^{D-1}(\xi) = \{\mathbf{x} \in \mathbb{R}^D \mid \|\mathbf{x}\|_2 = \xi\}$ is a $(D - 1)$ -sphere (i.e. a sphere in \mathbb{R}^D space) with radius $\xi \in \mathbb{R}^+$. \odot is element-wise product.

3 Method

3.1 Human Demonstration to Dexterous Robot Expert Policy

Recent works [1, 16] have shown success in learning five-finger dexterous robot policy from human hand demonstrations in diverse modalities, such as sensor glove signals [1] and visual data [16], which made the first step of our proposed paradigm possible. Inspired by this research progress, we adopt similar approaches to train expert policies on a dexterous robot as illustrated in Figure 1(1)(2).

Sensor Glove Demonstration When recorded in sensor glove signals, human demonstrations are directly converted to states and actions in a simulator [19] from which a policy is trained with algorithms such as DAPG [1]. We use the same procedure and obtain the expert policy as in [1].

Visual Demonstration We develop a toolchain for training dexterous policies from human visual demonstrations of manipulation. Our toolchain includes human and object pose estimation with visual perception followed by pose fitting of the dexterous robot via inverse kinematics (IK). We then train the policy by setting the episodes' initial state to be the state of the grasping frame, including poses and joint velocity. During training, the initial state gradually moves backward in time until the desired starting state. For more details, please refer to the supplementary.

3.2 Continuous Dexterous Hand to Target Commercial Robots Evolution

A core hypothesis in our proposed paradigm of learning from human demonstration is the feasibility of interpolation between a human-hand-like five-finger dexterous robot and a target commercial robot. In this paper, we present solutions for dexterous-to-commercial-robot interpolation for two target commercial robots to show this. Since both the dexterous hand robot and the target robots are complicated in structure, how to design the evolution from the former to the latter is not straightforward and has a large design space. The design choice can significantly affect the policy transfer performance. Following [18], we first match the robot morphology between the dexterous and the target robot. With the same morphology, we then design a shared high-dimensional robot parameter space that allows defining an intermediate robot by simply setting these parameters. The evolution includes both the dexterous hand and arm.

Dexterous Hand to Commercial Gripper Evolution To match the number of fingers, we keep the thumb and gradually shrink the redundant fingers to be zero-size and zero-mass so that they eventually disappear. We also gradually change the range of the finger joints to match the desired

joint configuration. In addition, we add new position servo joints to the remaining fingers. The position servo joints are initially frozen and evolve to have the same range as the target fingers.

Dexterous Arm to Commercial Robot Arm Evolution A major challenge of arm evolution is the different ways of arm mounting. In simulation, the dexterous robot elbow joint is usually modeled as a virtual free joint that can move freely in the 3D space, while the commercial robot arms are usually mounted on fixed bases. Another challenge is the huge difference in the numbers of arm joints and joint physical parameters. Our solution is to attach the free joint of the dexterous arm to the end effector of the target robot and treat the entire dexterous robot as a *de facto* large gripper. During evolution, both the dexterous arm and the elbow free joint gradually shrink to zero so that the dexterous robot eventually evolves to be firmly attached to the target robot end effector.

Our robot evolution solution includes the changing of D independent robot parameters such as body sizes and mass, and joint ranges and damping, where $D = 40$ for target Sawyer robot and $D = 42$ for target Jaco robot. The evolution process for Sawyer robot is illustrated in Figure 2.

3.3 Multi-dimensional Continuous Robot Evolution for Policy Transfer

As shown in Section 3.2, the evolution from a human-like dexterous robot to a target commercial robot is an extremely high-dimensional problem in robot parameter space (e.g. $D = 42$). This means there exist numerous choices of intermediate robot sequences that connect source to target robots. However, previous work REvolveR [18] assumes the same and uniform evolution progress hard-coded for all robot parameters and could be sub-optimal. We envision that when transferring the policy through intermediate robots, the optimal robot evolution should be flexible and able to smartly bypass difficult robot configurations to reach the target robot efficiently. In this section, we introduce an algorithm for automatically finding such optimized evolution strategy. We formulate the problem as a joint optimization of both robot evolution and the policy.

Problem Statement Suppose the source and target robot morphology is matched using the method in [18] or Section 3.2. Therefore the D kinematics parameters of the source and target robots can be mapped to the same space denoted as $\theta_S, \theta_T \in \mathbb{R}^D$. Continuous function $F : [0, 1]^D \rightarrow \mathcal{M}$ defines an intermediate robot by interpolation between all pairs of kinematic parameters $\theta = (\mathbf{1} - \alpha) \odot \theta_S + \alpha \odot \theta_T$ where $\alpha \in [0, 1]^D$ is the *evolution parameter* that describes the evolution progress of each of the D kinematics parameters. Given an expert policy $\pi_{F(\mathbf{0})}^*$ on the source robot $F(\mathbf{0})$, the overall goal is to find the optimal policy $\pi_{F(\mathbf{1})}^*$ on target robot $F(\mathbf{1})$. Note that the formulation of REvolveR [18] is a special case of our problem setting with $\alpha = \alpha \cdot \mathbf{1}$ and $\alpha \in [0, 1]$.

Differentiable Evolution Path Search (DEPS) We adopt multi-dimensional robot evolution as a solution to the above problem as illustrated in Figure 3(a). Suppose there is a robot evolution path $\tau = (F(\alpha_0), F(\alpha_1), F(\alpha_2), \dots, F(\alpha_{K-1}), F(\alpha_K))$ where $\alpha_0 = \mathbf{0}, \alpha_K = \mathbf{1}$. In k -th phase, the policy optimization objective is to maximize the expected reward $\mathbb{E}[\rho^{\pi, F(\alpha_k)}]$ on robot $F(\alpha_k)$. For all k , the evolution parameter step size $\xi = \|\alpha_k - \alpha_{k+1}\|_2$ is sufficiently small. In this way, we decompose the difficult robot-to-robot policy transfer problem into a sequence of K easy problems.

The optimal solution to the above problem requires finding the optimal evolution path τ together with policy optimization. We propose an algorithm named Differentiable Evolution Path Search (DEPS) to find both the optimized robot evolution path τ in tandem with policy optimization. Given the current evolution parameter α_k , we aim to find the next best evolution parameter $\alpha_{k+1} = \alpha_k + \mathbf{l}_k$ as well as its optimal policy $\pi_{F(\alpha_{k+1})}^*$. The optimization objective is formulated as

$$\max_{\mathbf{l}_k, \|\mathbf{l}_k\|_2 = \xi} \max_{\pi} L = \mathbb{E}[\rho^{\pi, F(\alpha_k + \mathbf{l}_k)}] - \frac{1}{2} \lambda \|\mathbf{1} - (\alpha_k + \mathbf{l}_k)\|_2^2 \quad (1)$$

where $\lambda \in \mathbb{R}^+$ is a weighting factor. The first term optimizes the policy reward while the second term encourages the evolved robot to move close to the target robot. Since step size ξ is small, we assume L is locally differentiable w.r.t. \mathbf{l}_k . Then the direction of \mathbf{l}_k can be estimated by

$$\mathbf{l}_k \approx \nabla_{\alpha} L = \nabla_{\alpha} \mathbb{E}[\rho^{\pi, F(\alpha)}] \Big|_{\alpha = \alpha_k} + \lambda(\mathbf{1} - \alpha_k) = \mathbf{J} + \lambda(\mathbf{1} - \alpha_k) \quad (2)$$

where $\mathbf{J} = \nabla_{\alpha} \mathbb{E}[\rho^{\pi, F(\alpha)}]$ is the Jacobian of expected reward w.r.t. evolution parameter α . The Jacobian \mathbf{J} can be estimated by finite difference with Monte-Carlo sampling of α . Concretely, we sample n random vectors $\delta_1, \delta_2, \dots, \delta_n$ with ℓ^2 -norm of ξ . Suppose $\delta_0 = \mathbf{0}$. For each δ_i , we

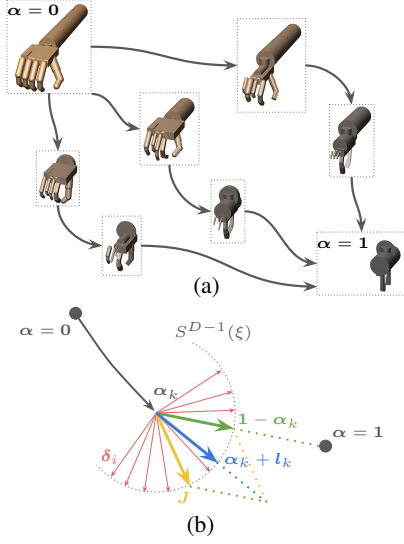


Figure 3: (a) Possible robot evolution paths from source to target robot. (b) Computation of the next evolution parameter $\alpha_{k+1} = \alpha_k + l_k$ in the path.

Algorithm 1 Multi-dimensional Robot Evolution Policy Transfer

1: **Notation Summary:**

2: $\alpha \in [0, 1]^D$: robot evolution parameter; $F : [0, 1]^D \rightarrow \mathcal{M}$: continuous robot evolution function; $\pi_{F(\mathbf{0})}$: expert policy on the source robot; $\xi \in \mathbb{R}^+$: evolution step size; $q \in \mathbb{R}$: reward threshold; $\lambda \in \mathbb{R}^+$: weight factor; $\lambda_1 \in (0, 1)$: shrink ratio;

3: $\alpha \leftarrow \mathbf{0}, \pi \leftarrow \pi_{F(\mathbf{0})}, \mathbf{l} \sim S^{D-1}(\xi)$ // initialization
4: **while** $\alpha \neq \mathbf{1}$ **do**
5: **if** $\mathbb{E}[\rho^{\pi, F(\alpha + \mathbf{l})}] < q$ **then**
6: $\delta_1, \delta_2, \dots, \delta_n \sim S^{D-1}(\xi), \delta_0 \leftarrow \mathbf{0}$ // sample δ_i vectors
7: execute π and $\rho_i \leftarrow \rho^{\pi, F(\alpha + \delta_i)}, \forall i \in \{0, \dots, n\}$
8: compute Jacobian \mathbf{J} from δ_j and ρ_j according to Eq.(4)
9: $\mathbf{l} \leftarrow \mathbf{J} / \|\mathbf{J}\|_2 + \lambda(\mathbf{1} - \alpha) / \|\mathbf{1} - \alpha\|_2$
10: $\mathbf{l} \leftarrow \mathbf{l} / \|\mathbf{l}\|_2 \cdot \xi$
11: **for** e in $0, 1, \dots, N_e$ **do**
12: $\beta \sim \text{Uniform}(1 - \lambda_1^e, 1)$
13: sample rollouts and train π on robot $F(\alpha + \beta \cdot \mathbf{l})$
14: **end for**
15: **end if**
16: $\alpha \leftarrow \min\{\max\{\alpha + \mathbf{l}, \mathbf{0}\}, \mathbf{1}\}$ // make sure stay in $[0, 1]$
17: **end while**
18: **return** π

execute π on robot $F(\alpha_k + \delta_i)$ to get episode reward $\rho_i = \rho^{\pi, F(\alpha_k + \delta_i)}$. By the definition of Jacobian, if there were no noise, ideally we should have

$$\mathbf{J} \cdot \delta_i = \rho^{\pi, F(\alpha_k + \delta_i)} - \rho^{\pi, F(\alpha_k)} = \rho_i - \rho_0, \quad \forall i \quad (3)$$

However, there is usually inevitable noise in the policy rollout and ρ_i . Let $\boldsymbol{\rho} = [\rho_1, \rho_2, \dots, \rho_n]^\top$ and $\boldsymbol{\Delta} = [\delta_1, \delta_2, \dots, \delta_n]$. The gradient can be estimated by Least Squares Minimization

$$\mathbf{J} \approx (\boldsymbol{\Delta}^\top \boldsymbol{\Delta})^{-1} \boldsymbol{\Delta}^\top (\boldsymbol{\rho} - \rho_0 \cdot \mathbf{1}) \quad (4)$$

Since the scale of the episode reward $\rho^{\pi, F(\alpha)}$ and therefore \mathbf{J} is task-dependent and can be arbitrary, to stabilize the evolution path search we scale both \mathbf{J} and $\mathbf{1} - \alpha_k$ in Equation (2) to be unit vectors to obtain the direction of evolution progression as follows

$$\mathbf{l}_k = \mathbf{J} / \|\mathbf{J}\|_2 + \lambda(\mathbf{1} - \alpha_k) / \|\mathbf{1} - \alpha_k\|_2 \quad (5)$$

The next evolution parameter is obtained by $\alpha_{k+1} = \alpha_k + \xi \cdot \mathbf{l}_k / \|\mathbf{l}_k\|_2$, where ξ is the evolution step size. The geometric interpretation of Equation (5) is illustrated in Figure 3(b).

We point out that the optimization objectives of our DEPS in Equations (2) and (5) can be viewed as a generalization of multiple previous works. When $\lambda \rightarrow +\infty$, the problem reduces to vanilla REvolveR [18] where $\alpha = \alpha \cdot \mathbf{1}$; when $\lambda \rightarrow 0$, the problem reduces to unrestricted robot and policy joint optimization such as [20] and [21]. Note that when $\lambda > 1$, $\{\alpha_k\}_k$ is guaranteed to converge to $\mathbf{1}$, because it is easy to show for all \mathbf{l} with ℓ^2 -norm of ξ , $\|\mathbf{1} - (\alpha_{k+1} + \mathbf{l})\|_2 \leq \|\mathbf{1} - \alpha_k\|_2 - \xi|\lambda - 1|$.

Policy Optimization along the Evolution Path Given the next evolution parameter $\alpha_{k+1} = \alpha_k + \mathbf{l}_k$ and the optimized policy $\pi_{F(\alpha_k)}$, the next goal is to find the optimal policy $\pi_{F(\alpha_{k+1})}^*$ on robot $F(\alpha_{k+1})$. Instead of directly fine-tuning $\pi_{F(\alpha_k)}$ on α_{k+1} , we adopt the following optimization objective with randomized evolution progression similar to [18] to achieve the goal:

$$\pi_{F(\alpha_{k+1})} = \arg \max_{\pi} \mathbb{E}_{\beta \sim \text{Uniform}(1 - \lambda_1^e, 1)} \rho^{\pi, F(\alpha_k + \beta \cdot \mathbf{l}_k)} \quad (6)$$

where $\lambda_1 \in (0, 1)$ is the ratio of range shrinkage and $e \in \mathbb{N}$ is the iteration counter. The above optimization objective allows the policy to be fine-tuned on a set of randomly sampled robots within a range along the \mathbf{l}_k to improve the stability and robustness of training while also ensuring the sampled evolution parameter α to converge to $\alpha_{k+1} = \alpha_k + \mathbf{l}_k$ when $e \rightarrow +\infty$. In practice, a batch of β in Equation (6) is sampled in each iteration. The overall algorithm is illustrated in Algorithm 1.

4 Related Work

Learning from Human Demonstration Human demonstrations are often collected in terms of trajectories that could be obtained by teleoperation via virtual reality, motion capture markers, or kinesthetic control of robot. A policy is then learned by cloning the demonstrations [22, 23, 24, 25, 26, 27] or through inverse reinforcement learning [25, 28, 29, 30, 31]. In contrast to these methods, in our approach, the human does not control the robot to which the demonstration is transferred.

Human demonstrations need not always be in the form of state space information and a recent line of work rely on visual demonstration to enhance the scalability of data collection as it is much easier to watch humans than ask them to collect demos [32, 33, 34, 35, 36, 37, 38, 39, 40, 41]. Although in our case, the demonstrations are converted to the state space of the dexterous hand robot through inverse kinematics, they are originally collected by watching humans. Different from these prior works, we use the demonstration to transfer the policy to very different robots than the demonstrator.

Learning Controllers for New Robot Morphology Evolutionary methods to get new shapes date back to the early days of automata theory from Von Neumann [42]. In early 90s, Karl Sims showed the effectiveness of evolutionary methods in optimizing robot shapes and controllers [43, 44]. These works laid the foundation of the area where not only robots are optimized but also controllers are transferred across evolved robots. In recent years, many works have revived this idea using deep learning based graph evolution [45, 46, 47, 48, 49]. Our work does not treat the morphological evolution in the form of graph networks but rather gradually morphs the source robot to target robot.

Relation to Path Planning Our robot evolution path search problem is similar to the problem of path planning [50, 51, 52, 53, 54, 55]. However, unlike ordinary planning where the obstacles are known, in our problem the difficult robot configurations are unknown. Moreover, in ordinary path planning, evaluating the cost of a path is cheap, while in our case, transferring the policy to a new robot requires a large number of policy optimization iterations and is computationally costly.

5 Experiments

Our experiment is designed to verify the following two hypotheses: (1) our proposed DEPS algorithm can find optimized evolution paths in high-dimensional robot parameter space to improve policy transfer over vanilla linear evolution path [18]; (2) our HERD framework can learn from human demonstrations recorded in diverse modalities including sensor glove signal and visual data.

Experiment Settings We conduct experiments in MuJoCo physics simulation engine [56]. We adopt the five-finger dexterous hand robot provided in the ADROIT platform [57]. The high-fidelity models of the target robots and grippers are imported from robosuite environment [58] and have been used in previous robotics publications that eventually transferred their experiments to real robots such as [59, 60]. We use NPG [61] as the RL algorithm for policy optimization. Due to the nature of robot-to-robot policy transfer, the total number of RL iterations it takes to reach the goal of a certain success rate or episode reward cannot be set beforehand. So we instead report the number of policy training iterations and simulation epochs needed to reach 80% success rate on the tasks.

5.1 Learning from Sensor Glove Signal Demonstrations

Tasks and Demonstrations We use the three tasks from the Hand Manipulation Suite (HMS) [1]: Hammer, Relocate, and Door. In Hammer, the task is to pick up the hammer and smash the nail into the board; In Relocate, the task is to pick up the ball and move it to the target position; In Door, the task is to turn the door handle and fully open the door. We use a sparse reward setting where only task completion is rewarded. For each task, HMS [1] provided 25 human demonstrations recorded as palm and finger locations using a sensor glove named CyberGlove III. Then the expert policy on the dexterous robot is trained using DAPG [1].

Qualitative Results We provide visualization of the policies on the intermediate robots learned during evolution with our HERD in Figure 4. Starting from the dexterous robot, our proposed DEPS algorithm is able to find the next optimized evolved robot. The policy is also able to iteratively adapt to new evolved robots and successfully transfer to the target robots.

Quantitative Comparison with Baselines We compare our HERD against the following baseline methods for learning a policy on the target robot: (1) *From Scratch*: we train policy on the target robot from scratch with the RL algorithm under both sparse and dense shaped rewards; (2) *DAPG*

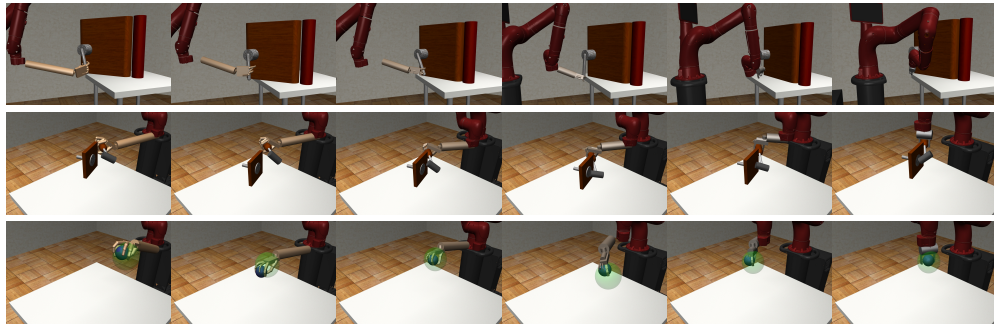


Figure 4: **Visualization of policies on evolving intermediate robots on Hand Manipulation Suite tasks [1].** We show the results of the learned policies on Door, Hammer and Relocate tasks in three rows respectively. Zoom in for better view.

	Reward	Demo Agent	Door		Hammer		Relocate	
			# of sim epochs	# of train iters	# of sim epochs	# of train iters	# of sim epochs	# of train iters
From Scratch	Shaped	None	608700 \pm 79410	50725 \pm 6617	248460 \pm 9732	20705 \pm 811	693540 \pm 118860	57795 \pm 9905
	Sparse	None	∞	∞	∞	∞	∞	∞
DAPG [1]	Sparse	Sawyer	245659 \pm 24934	20471 \pm 2077	161047 \pm 14027	13420 \pm 1168	114335 \pm 15343	9527 \pm 1278
REvolveR [18]	Sparse	ADROIT	273663 \pm 28236	14302 \pm 1843	110198 \pm 4407	6356 \pm 274	163611 \pm 2859	8808 \pm 450
HERD (Ours)	Sparse	ADROIT	201190 \pm 23466	11229 \pm 1166	91674 \pm 6557	4434 \pm 605	145158 \pm 4207	8294 \pm 1265

(a) Performance with Sawyer robot as the target robot.

	Reward	Demo Agent	Door		Hammer		Relocate	
			# of sim epochs	# of train iters	# of sim epochs	# of train iters	# of sim epochs	# of train iters
REvolveR [18]	Sparse	ADROIT	367612 \pm 48859	17652 \pm 2915	220169 \pm 20262	11626 \pm 509	259387 \pm 2641	13215 \pm 223
HERD (Ours)	Sparse	ADROIT	335196 \pm 17938	13398 \pm 2616	206214 \pm 6576	8810 \pm 390	214200 \pm 5108	10179 \pm 704

(b) Performance with Jaco robot as the target robot.

Table 1: **Experiments on Hand Manipulation Suite tasks [1].** The evaluation metrics is the number of simulation epochs and policy optimization iterations needed to reach 80% task success rate, shown as the “mean \pm standard deviation” from runs with 5 random seeds.

[1]: a variant of NPG [61] with demonstration-augmented policy gradient. We use the rollouts of transferred HERD policy on the target robots as the demonstrations for DAPG; (3) *REvolveR* [18]: robot-to-robot policy transfer with continuous and linear robot evolution path which is a special case of our HERD. The results are illustrated in Table 1.

Training RL from scratch never completes the task to receive reward and is not able to learn on these tasks. Robot-to-robot evolution solutions with sparse rewards are able to successfully transfer the policy and even significantly outperform training from scratch with shaped rewards. Moreover, our HERD outperforms *REvolveR* [18], though the margin in simulation epochs is smaller than RL iterations in that HERD spends additional simulation epochs to obtain Jacobian as in Equation (4). We notice that our HERD also has advantage over DAPG trained using expert rollouts directly collected on the target robot. This shows that training a policy while maintaining sufficient reward/success during robot evolution has advantage over exploration from scratch even with demonstration.

5.2 Learning From Visual Demonstrations

Task and Demonstrations In addition to the demonstration captured by sensor glove, we are also interested in showing learning from visual human demonstration with our HERD. We use DexYCB dataset [2] as the source of human demonstration. DexYCB dataset is a multi-view RGB-D video dataset capturing human hand manipulating YCB objects [62]. We define the task as grasping and then moving the object of interest to the desired position within a distance threshold as demonstrated in the DexYCB videos. We use 5 YCB objects in Table 2. For each object, we take one video which results in 5 demonstrations in total. The human hand joint poses and object 6D poses are estimated by HRNet32 [63] and CozyPose [64] respectively. Then the expert dexterous policy is trained using the method in Section 3.1. The reward is sparse task completion reward.

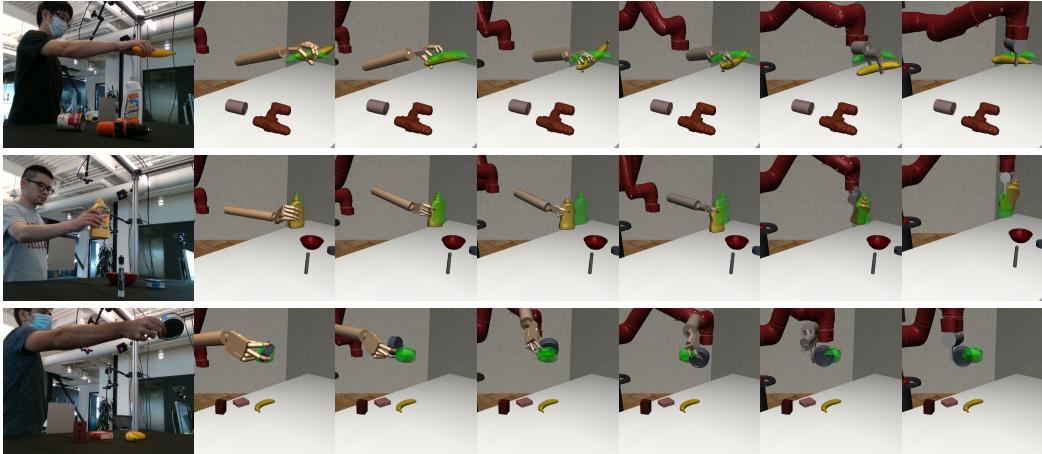


Figure 5: **Visualization of policies on evolving intermediate robots on DexYCB dataset manipulations [2].** The target robot is Sawyer. We show the results of manipulation policies learned from human demonstration on 011_banana, 006_mustard_bottle and 007_tuna_fish_can in three rows respectively.

YCB Objects	REvolveR [18]		HERD (Ours)	
	# of sim epochs	# of train iters	# of sim epochs	# of train iters
006_mustard_bottle	279563 \pm 20115	25645 \pm 2181	253920 \pm 22745	19361 \pm 1799
007_tuna_fish_can	320951 \pm 14466	29812 \pm 1569	286550 \pm 33816	23165 \pm 2693
008_pudding_box	306532 \pm 17388	28537 \pm 1522	264512 \pm 32775	22866 \pm 2986
011_banana	52094 \pm 2288	4797 \pm 262	51811 \pm 3490	4022 \pm 349
025_bowl	817255 \pm 46721	73799 \pm 3892	725919 \pm 59419	65957 \pm 5105

Table 2: **Experiments on the DexYCB dataset [2].** The target robot is Sawyer. The evaluation metrics is the number of simulation epochs and policy optimization iterations needed to reach task success, shown as the “mean \pm standard deviation” from runs with 5 random seeds.

Result Analysis and Comparison We compare against REvolveR [18] and illustrate the experiment results in Table 2. Our HERD outperforms REvolveR in terms of policy iterations as well as most reported simulation epoch metrics. One interesting finding is that the policy for manipulating 011_banana object is the easiest task among all objects. A possible reason is that 011_banana object has a geometry most suitable for both the dexterous hand and target gripper.

Qualitative Results We visualize the policies on the intermediate robots learned during evolution with our HERD in Figure 5. Again, our proposed DEPS algorithm is able to find the next optimized evolved robot while successfully transferring the policy to the target robot. For more details on the visualizations in this section, please refer to the supplementary video.

6 Conclusion

In this paper, we propose a framework named HERD for learning from human demonstration. HERD framework utilizes the continuous evolution of robots to transfer the expert policy from embodied dexterous hands to a target robot. We conduct experiments using the human demonstrations from Human Manipulation Suite [1] and DexYCB dataset [2]. We show that the proposed approach is able to transfer expert policy trained using human demonstrations in sensor glove signals or visual data to target two-finger Sawyer and three-finger Jaco robots, even with challenging sparse rewards.

Limitations We expect that our HERD would fail in learning from human demonstrations for robots with extremely different functions than humans, e.g. learning object manipulation policy for a robot arm mounted with a suction cup from human hand manipulation demonstrations. This is because our proposed human-to-robot continuous evolution solution can smoothly interpolate different morphology but cannot interpolate different functions of the robot end-effector. We leave the exploration of more general human-to-robot continuous evolution solutions as future work.

Acknowledgement This work is in part funded by JST AIP Acceleration, Grant Number JP-MJCR20U1, Japan. Deepak Pathak is supported by NSF grant IIS-2024594.

References

- [1] A. Rajeswaran, V. Kumar, A. Gupta, G. Vezzani, J. Schulman, E. Todorov, and S. Levine. Learning complex dexterous manipulation with deep reinforcement learning and demonstrations. In *Proceedings of Robotics: Science and Systems (RSS)*, Pittsburgh, Pennsylvania, June 2018. doi:10.15607/RSS.2018.XIV.049.
- [2] Y.-W. Chao, W. Yang, Y. Xiang, P. Molchanov, A. Handa, J. Tremblay, Y. S. Narang, K. Van Wyk, U. Iqbal, S. Birchfield, J. Kautz, and D. Fox. DexYCB: A benchmark for capturing hand grasping of objects. In *IEEE/CVF Conference on Computer Vision and Pattern Recognition (CVPR)*, 2021.
- [3] B. D. Argall, S. Chernova, M. Veloso, and B. Browning. A survey of robot learning from demonstration. *Robotics and autonomous systems*, 57(5):469–483, 2009.
- [4] D. Damen, H. Doughty, G. M. Farinella, S. Fidler, A. Furnari, E. Kazakos, D. Moltisanti, J. Munro, T. Perrett, W. Price, et al. Scaling egocentric vision: The epic-kitchens dataset. In *Proceedings of the European Conference on Computer Vision (ECCV)*, pages 720–736, 2018.
- [5] K. Grauman, A. Westbury, E. Byrne, Z. Chavis, A. Furnari, R. Girdhar, J. Hamburger, H. Jiang, M. Liu, X. Liu, M. Martin, T. Nagarajan, I. Radosavovic, S. K. Ramakrishnan, F. Ryan, J. Sharma, M. Wray, M. Xu, E. Z. Xu, C. Zhao, S. Bansal, D. Batra, V. Cartillier, S. Crane, T. Do, M. Doulaty, A. Erapalli, C. Feichtenhofer, A. Fragomeni, Q. Fu, C. Fuegen, A. Gebreselasie, C. Gonzalez, J. Hillis, X. Huang, Y. Huang, W. Jia, W. Khoo, J. Kolar, S. Kottur, A. Kumar, F. Landini, C. Li, Y. Li, Z. Li, K. Mangalam, R. Modhugu, J. Munro, T. Murrell, T. Nishiyasu, W. Price, P. R. Puentes, M. Ramazanova, L. Sari, K. Somasundaram, A. Southland, Y. Sugano, R. Tao, M. Vo, Y. Wang, X. Wu, T. Yagi, Y. Zhu, P. Arbelaez, D. Crandall, D. Damen, G. M. Farinella, B. Ghanem, V. K. Ithapu, C. V. Jawahar, H. Joo, K. Kitani, H. Li, R. Newcombe, A. Oliva, H. S. Park, J. M. Rehg, Y. Sato, J. Shi, M. Z. Shou, A. Torralba, L. Torresani, M. Yan, and J. Malik. Ego4d: Around the world in 3,000 hours of egocentric video. *arXiv preprint arXiv:2110.07058*, 2021.
- [6] S. Hampali, M. Rad, M. Oberweger, and V. Lepetit. Honnotate: A method for 3d annotation of hand and object poses. In *Proceedings of the IEEE/CVF conference on computer vision and pattern recognition*, pages 3196–3206, 2020.
- [7] T. Kwon, B. Tekin, J. Stühmer, F. Bogo, and M. Pollefeys. H2o: Two hands manipulating objects for first person interaction recognition. In *Proceedings of the IEEE/CVF International Conference on Computer Vision*, pages 10138–10148, 2021.
- [8] S. Ross, G. Gordon, and D. Bagnell. A reduction of imitation learning and structured prediction to no-regret online learning. In *Proceedings of the fourteenth international conference on artificial intelligence and statistics*, pages 627–635. JMLR Workshop and Conference Proceedings, 2011.
- [9] A. Y. Ng, S. J. Russell, et al. Algorithms for inverse reinforcement learning. In *Icml*, volume 1, page 2, 2000.
- [10] I. Radosavovic, X. Wang, L. Pinto, and J. Malik. State-only imitation learning for dexterous manipulation. *arXiv preprint arXiv:2004.04650*, 2020.
- [11] H. Xiong, Q. Li, Y.-C. Chen, H. Bharadhwaj, S. Sinha, and A. Garg. Learning by watching: Physical imitation of manipulation skills from human videos. *arXiv preprint arXiv:2101.07241*, 2021.
- [12] A. Bajcsy, D. P. Losey, M. K. O’Malley, and A. D. Dragan. Learning robot objectives from physical human interaction. In *Conference on Robot Learning*, pages 217–226. PMLR, 2017.
- [13] M. Li, A. Canberk, D. P. Losey, and D. Sadigh. Learning human objectives from sequences of physical corrections. In *2021 IEEE International Conference on Robotics and Automation (ICRA)*, pages 2877–2883. IEEE, 2021.

- [14] A. Mandlekar, Y. Zhu, A. Garg, J. Booher, M. Spero, A. Tung, J. Gao, J. Emmons, A. Gupta, E. Orbay, et al. Roboturk: A crowdsourcing platform for robotic skill learning through imitation. In *Conference on Robot Learning*, pages 879–893. PMLR, 2018.
- [15] Y. Qin, H. Su, and X. Wang. From one hand to multiple hands: Imitation learning for dexterous manipulation from single-camera teleoperation. *arXiv preprint arXiv:2204.12490*, 2022.
- [16] Y. Qin, Y.-H. Wu, S. Liu, H. Jiang, R. Yang, Y. Fu, and X. Wang. Dexmv: Imitation learning for dexterous manipulation from human videos. *arXiv preprint arXiv:2108.05877*, 2021.
- [17] F. Liu, Z. Ling, T. Mu, and H. Su. State alignment-based imitation learning. *arXiv preprint arXiv:1911.10947*, 2019.
- [18] X. Liu, D. Pathak, and K. M. Kitani. Revolver: Continuous evolutionary models for robot-to-robot policy transfer. *arXiv preprint arXiv:2202.05244*, 2022.
- [19] V. Kumar and E. Todorov. Mujoco haptix: A virtual reality system for hand manipulation. In *2015 IEEE-RAS 15th International Conference on Humanoid Robots (Humanoids)*, pages 657–663, 2015. doi:10.1109/HUMANOIDS.2015.7363441.
- [20] X. Pan, A. Garg, A. Anandkumar, and Y. Zhu. Emergent hand morphology and control from optimizing robust grasps of diverse objects. In *2021 IEEE International Conference on Robotics and Automation (ICRA)*, pages 7540–7547. IEEE, 2021.
- [21] Y. Yuan, Y. Song, Z. Luo, W. Sun, and K. Kitani. Transform2act: Learning a transform-and-control policy for efficient agent design. *arXiv preprint arXiv:2110.03659*, 2021.
- [22] D. A. Pomerleau. ALVINN: An autonomous land vehicle in a neural network. In *NIPS*, 1989.
- [23] B. D. Argall, S. Chernova, M. Veloso, and B. Browning. A survey of robot learning from demonstration. *Robotics and autonomous systems*, 2009.
- [24] S. Schaal. Is imitation learning the route to humanoid robots? *Trends in cognitive sciences*, 1999.
- [25] A. Y. Ng and S. J. Russell. Algorithms for inverse reinforcement learning. In *ICML*, pages 663–670, 2000.
- [26] B. Akgun, M. Cakmak, J. W. Yoo, and A. L. Thomaz. Trajectories and keyframes for kinesi-
thetic teaching: A human-robot interaction perspective. In *HRI*, March 2012.
- [27] T. Zhang, Z. McCarthy, O. Jow, D. Lee, K. Goldberg, and P. Abbeel. Deep imitation learning for complex manipulation tasks from virtual reality teleoperation. *CoRR*, abs/1710.04615, 2017.
- [28] P. Abbeel and A. Y. Ng. Apprenticeship learning via inverse reinforcement learning. In *ICML*, 2004.
- [29] B. D. Ziebart, A. Maas, J. A. Bagnell, and A. K. Dey. Maximum entropy inverse reinforcement learning. In *AAAI*, 2008.
- [30] S. Levine, P. Pastor, A. Krizhevsky, and D. Quillen. Learning hand-eye coordination for robotic grasping with large-scale data collection. In *ISER*, 2016.
- [31] J. Ho and S. Ermon. Generative adversarial imitation learning. In *NIPS*, 2016.
- [32] H. Koichi and H. Tom. *Visual servoing: real-time control of robot manipulators based on visual sensory feedback*, volume 7. World scientific, 1993.
- [33] B. H. Yoshimi and P. K. Allen. Active, uncalibrated visual servoing. In *Robotics and Automation, 1994. Proceedings., 1994 IEEE International Conference on*, pages 156–161. IEEE, 1994.
- [34] W. J. Wilson, C. W. Hulls, and G. S. Bell. Relative end-effector control using cartesian position based visual servoing. *IEEE Transactions on Robotics and Automation*, 12(5):684–696, 1996.

- [35] G. Caron, E. Marchand, and E. M. Mouaddib. Photometric visual servoing for omnidirectional cameras. *Autonomous Robots*, 35(2-3):177–193, 2013.
- [36] P. Sermanet, C. Lynch, Y. Chebotar, J. Hsu, E. Jang, S. Schaal, and S. Levine. Time-contrastive networks: Self-supervised learning from video. In *ICRA*, 2018.
- [37] P. Sharma, D. Pathak, and A. Gupta. Third-person visual imitation learning via decoupled hierarchical controller. *arXiv preprint arXiv:1911.09676*, 2019.
- [38] Y. Liu, A. Gupta, P. Abbeel, and S. Levine. Imitation from observation: Learning to imitate behaviors from raw video via context translation. *ICRA*, 2018.
- [39] L. Smith, N. Dhawan, M. Zhang, P. Abbeel, and S. Levine. Avid: Learning multi-stage tasks via pixel-level translation of human videos. In *RSS*, 2020.
- [40] D. Pathak, P. Mahmoudieh, G. Luo, P. Agrawal, D. Chen, Y. Shentu, E. Shelhamer, J. Malik, A. A. Efros, and T. Darrell. Zero-shot visual imitation. In *ICLR*, 2018.
- [41] J.-Y. Zhu, T. Park, P. Isola, and A. A. Efros. Unpaired image-to-image translation using cycle-consistent adversarial networks. *ICCV*, 2017.
- [42] J. Von Neumann, A. W. Burks, et al. Theory of self-reproducing automata. *IEEE Transactions on Neural Networks*, 1966.
- [43] K. Sims. Evolving virtual creatures. In *Computer graphics and interactive techniques*, 1994.
- [44] K. Sims. Evolving 3d morphology and behavior by competition. *Artificial life*, 1994.
- [45] D. Pathak, C. Lu, T. Darrell, P. Isola, and A. A. Efros. Learning to control self-assembling morphologies: a study of generalization via modularity. *NeurIPS*, 2019.
- [46] T. Wang, R. Liao, J. Ba, and S. Fidler. Nervenet: Learning structured policy with graph neural networks. *ICLR*, 2018.
- [47] T. Wang, Y. Zhou, S. Fidler, and J. Ba. Neural graph evolution: Towards efficient automatic robot design. *arXiv preprint arXiv:1906.05370*, 2019.
- [48] D. J. Hejna III, P. Abbeel, and L. Pinto. Task-agnostic morphology evolution. *arXiv preprint arXiv:2102.13100*, 2021.
- [49] A. Gupta, S. Savarese, S. Ganguli, and L. Fei-Fei. Embodied intelligence via learning and evolution. *arXiv preprint arXiv:2102.02202*, 2021.
- [50] S. LAVALLE. Rapidly-exploring random trees: A new tool for path planning. *Computer Science Dept. Oct.*, 98(11), 1998.
- [51] S. Karaman and E. Frazzoli. Sampling-based algorithms for optimal motion planning. *The international journal of robotics research*, 30(7):846–894, 2011.
- [52] F. Islam, J. Nasir, U. Malik, Y. Ayaz, and O. Hasan. Rrt*-smart: Rapid convergence implementation of rrt* towards optimal solution. In *2012 IEEE international conference on mechatronics and automation*, pages 1651–1656. IEEE, 2012.
- [53] A. Perez, R. Platt, G. Konidaris, L. Kaelbling, and T. Lozano-Perez. Lqr-rrt*: Optimal sampling-based motion planning with automatically derived extension heuristics. In *2012 IEEE International Conference on Robotics and Automation*, pages 2537–2542. IEEE, 2012.
- [54] P. E. Hart, N. J. Nilsson, and B. Raphael. A formal basis for the heuristic determination of minimum cost paths. *IEEE transactions on Systems Science and Cybernetics*, 4(2):100–107, 1968.
- [55] S. Koenig, M. Likhachev, and D. Furcy. Lifelong planning a*. *Artificial Intelligence*, 155(1-2): 93–146, 2004.

- [56] E. Todorov, T. Erez, and Y. Tassa. Mujoco: A physics engine for model-based control. In *2012 IEEE/RSJ International Conference on Intelligent Robots and Systems*, pages 5026–5033. IEEE, 2012.
- [57] V. Kumar, Z. Xu, and E. Todorov. Fast, strong and compliant pneumatic actuation for dexterous tendon-driven hands. In *2013 IEEE international conference on robotics and automation*, pages 1512–1519. IEEE, 2013.
- [58] Y. Zhu, J. Wong, A. Mandlekar, and R. Martín-Martín. robosuite: A modular simulation framework and benchmark for robot learning. In *arXiv preprint arXiv:2009.12293*, 2020.
- [59] W. Zhou and D. Held. Learning to grasp the ungraspable with emergent extrinsic dexterity. In *ICRA 2022 Workshop: Reinforcement Learning for Contact-Rich Manipulation*, 2022.
- [60] Z. Jiang, C.-C. Hsu, and Y. Zhu. Ditto: Building digital twins of articulated objects from interaction. In *Proceedings of the IEEE/CVF Conference on Computer Vision and Pattern Recognition*, pages 5616–5626, 2022.
- [61] A. Rajeswaran, K. Lowrey, E. Todorov, and S. Kakade. Towards generalization and simplicity in continuous control. *arXiv preprint arXiv:1703.02660*, 2017.
- [62] Y. Xiang, T. Schmidt, V. Narayanan, and D. Fox. Posecnn: A convolutional neural network for 6d object pose estimation in cluttered scenes. *arXiv preprint arXiv:1711.00199*, 2017.
- [63] A. Spurr, U. Iqbal, P. Molchanov, O. Hilliges, and J. Kautz. Weakly supervised 3d hand pose estimation via biomechanical constraints. In *Computer Vision—ECCV 2020: 16th European Conference, Glasgow, UK, August 23–28, 2020, Proceedings, Part XVII 16*, pages 211–228. Springer, 2020.
- [64] Y. Labbé, J. Carpentier, M. Aubry, and J. Sivic. Cosypose: Consistent multi-view multi-object 6d pose estimation. In *European Conference on Computer Vision*, pages 574–591. Springer, 2020.
- [65] M. J. Powell. An efficient method for finding the minimum of a function of several variables without calculating derivatives. *The computer journal*, 7(2):155–162, 1964.
- [66] Y.-H. Wu, J. Wang, and X. Wang. Learning generalizable dexterous manipulation from human grasp affordance. *arXiv preprint arXiv:2204.02320*, 2022.
- [67] C. Florensa, D. Held, M. Wulfmeier, M. Zhang, and P. Abbeel. Reverse curriculum generation for reinforcement learning. In *Conference on robot learning*, pages 482–495. PMLR, 2017.
- [68] A. Paszke, S. Gross, F. Massa, A. Lerer, J. Bradbury, G. Chanan, T. Killeen, Z. Lin, N. Gimelshein, L. Antiga, et al. Pytorch: An imperative style, high-performance deep learning library. *Advances in neural information processing systems*, 32, 2019.
- [69] C. Liu, B. Zoph, M. Neumann, J. Shlens, W. Hua, L.-J. Li, L. Fei-Fei, A. Yuille, J. Huang, and K. Murphy. Progressive neural architecture search. In *Proceedings of the European conference on computer vision (ECCV)*, pages 19–34, 2018.
- [70] H. Liu, K. Simonyan, and Y. Yang. Darts: Differentiable architecture search. *arXiv preprint arXiv:1806.09055*, 2018.
- [71] S. Cao, X. Wang, and K. M. Kitani. Learnable embedding space for efficient neural architecture compression. In *International Conference on Learning Representations*, 2018.

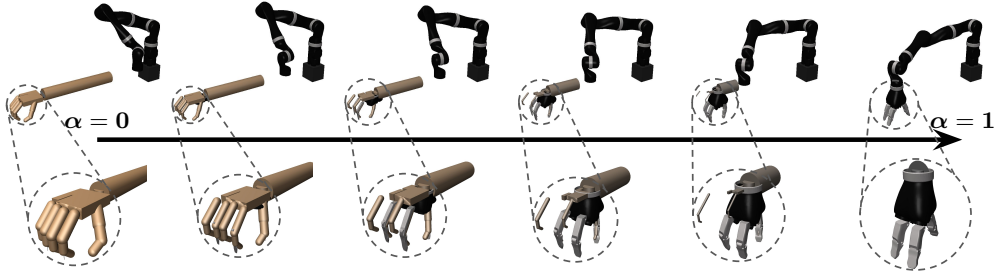


Figure 6: **Continuous hand-to-robot evolution for Jaco robot.** We show one evolution path from human dexterous hand ($\alpha = 0$) to a commercial Jaco robot with three-finger Jaco gripper ($\alpha = 1$). From left to right, we show intermediate robots along the path. Zoom in for better view.

A Overview

In this document, we provide additional information as presented in the main paper. We present additional technical details of our solution to human-to-robot continuous evolution in Section B. We introduce our proposed method for learning expert dexterous robot policy from human visual demonstration in Section C. We provide details on the hyperparameter settings of our experiments in Section D. Lastly, in Section E, we discuss further on related works and problems.

B Details on Hand-to-Robot Continuous Evolution

Virtual Confinement of the Robot End Effector The implementation of the dexterous hand robot simulation usually assumes the elbow is able to move freely in all 6 degrees. This is modeled as the elbow being connected by six virtual joints that are attached to a fixed mount point in space. However, in our solution of human-to-robot evolution, the elbow of the dexterous robot is modeled as being connected to the robot end effector. If the robot end effector is also allowed to move freely at the start of the evolution, a well-trained policy on the original dexterous robot will be ruined by the motion of the robot end effector, because the original policy assumes that the virtual joints are mounted to a fixed base. The policy transfer will fail even before the training on the continuously evolving robots starts.

We propose a mechanism named *virtual confinement* to address this. Virtual confinement exerts restrictions on the motion range of the robot end effector. At the start of the evolution, the allowed motion range of the robot end effector in all degrees of freedom is set to 0 which means the robot end effector is completely frozen. This means the virtual free joints of the dexterous hand robot are equivalently still mounted on a fixed base so that the original dexterous hand robot expert policy can be seamlessly imported to the combined robot. The motion range of the robot end effector gradually increases with the evolution progress and eventually allows the robot to move freely in the space of the environment. The virtual confinement does not correspond to any entity in the simulation environment but is modeled as several virtual joints mounted in a virtual base in space. The position of the virtual base is the same as the initial position of the robot end effector. The restriction on the motion range of the virtual joints can be implemented by the `equality` mechanism in MuJoCo Engine [56]. We use the proposed virtual confinement mechanism in all experiments in the main paper. The virtual confinement mechanism is illustrated in Figure 7.

Gripper Finger Synchronization The fingers of commercial robot grippers are usually synchronized in motion as position servo so that the grasping action is controlled by a single signal. On the other hand, the motion of the human hand fingers are asynchronous and independent from each other. To interpolate such behavior, we add additional position servo joints to the human hand. During robot evolution from human hand to the target robot, the motion range of the position servos gradually increase while the range of the independent joints gradually shrink to zero.

Disabling Collision Since the Sawyer robot end effector is not originally designed to be mounted with a dexterous hand robot, it is likely that the dexterous hand robot and the target Sawyer robot can collide during simulation unexpectedly and cause unstable behavior. Therefore, during simulation, we manually disable all pairs of collisions between the human hand bodies and robot bodies. Disabling collisions can be implemented by the `exclude` mechanism in MuJoCo Engine [56].

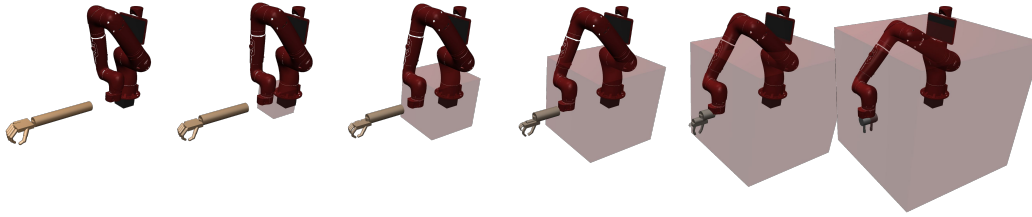


Figure 7: **Continuous evolution of the virtual confinement of the robot end effector.** The red semitransparent 3D box denotes the 3D space that the robot end effector is allowed to move to. Initially the end effector is completely frozen in its motion. The allowed 6D motion range gradually increases with evolution.

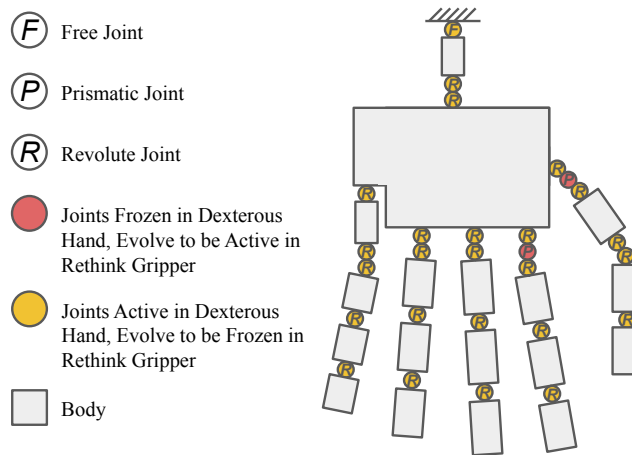


Figure 8: **Kinematic tree of dexterous hand robot.** All **revolute and free joints** will gradually freeze during evolution. The two **prismatic joints** are initially frozen and evolve to be active.

Human-to-robot Evolution Specifics We illustrate the kinematic tree of the dexterous hand robot in Figure 8. For Sawyer robot with Rethink gripper, during evolution, all revolute joints and the elbow free joint gradually freeze to have a range of 0. On the other hand, the two synchronized prismatic joints are initially frozen with a range of 0, and their range gradually increases until the same full range as the Rethink gripper. During the evolution, all bodies of the middle finger, ring finger and little finger gradually shrink to zero-size and disappear. The shapes of the bodies of the first finger, thumb and palm change continuously and become the same shape as the Rethink gripper eventually. The robot parameters of the Sawyer robot where the dexterous hand robot is attached to are not changed, except the range of virtual confinement which has the same evolution progress as the `elbow_joint_range`.

The evolution process for the three-finger Jaco robot is slightly different from Sawyer. In Jaco robot, the synchronized prismatic joints are the three revolute joints of the gripper. In order to model the interpolation of the synchronized joints, similar to Sawyer robot solution, we add three additional synchronized position servo joints. The three synchronized revolute joints are initially frozen with a range of 0, and their range gradually increases until the same full range of the Jaco gripper. The evolution process for Jaco robot is illustrated in Figure 6.

As mentioned in the main paper, our evolution solution includes the changing of D independent robot parameters where $D = 40$ for Sawyer robot and $D = 42$ for Jaco robot. We illustrate the robot parameters in Tables 3 and 4. The changing robot parameters include body shapes and mass, and joint ranges and damping etc. The ranges of all changes in robot parameters are linearly normalized to $[0, 1]$ so that we can map the evolution progress of robot parameters to $[0, 1]^D$.

ID	Robot Parameter	ID	Robot Parameter	ID	Robot Parameter
1	th_proximal_length	15	lf_distal_length	29	mf_shape
2	th_middle_length	16	th_joint_4_range	30	rf_shape
3	th_distal_length	17	th_joint_3_range	31	lf_shape
4	ff_proximal_length	18	th_joint_2_range	32	th_knuckle_position
5	ff_middle_length	19	th_joint_1_range	33	ff_knuckle_position
6	ff_distal_length	20	th_joint_0_range	34	mf_knuckle_position
7	mf_proximal_length	21	ff_joint_3_range	35	rf_knuckle_position
8	mf_middle_length	22	ff_joint_2_range	36	lf_knuckle_position
9	mf_distal_length	23	ff_joint_1_range	37	palm_shape
10	rf_proximal_length	24	ff_joint_0_range	38	wrist_joints
11	rf_middle_length	25	th_slide_joint	39	arm_length
12	rf_distal_length	26	ff_slide_joint	40	elbow_joint_range
13	lf_proximal_length	27	th_shape		
14	lf_middle_length	28	ff_shape		

Table 3: **Space of robot parameter evolution for two-finger Sawyer robot as target.** th, ff, mf, rt and lf represent thumb, first finger, middle finger, ring finger and little finger respectively. The robot evolution is described by $D = 40$ independent parameters in evolution in total.

ID	Robot Parameter	ID	Robot Parameter	ID	Robot Parameter
1	th_proximal_length	15	lf_distal_length	29	th_shape
2	th_middle_length	16	th_joint_4_range	30	ff_shape
3	th_distal_length	17	th_joint_3_range	31	mf_shape
4	ff_proximal_length	18	th_joint_2_range	32	rf_shape
5	ff_middle_length	19	th_joint_1_range	33	lf_shape
6	ff_distal_length	20	th_joint_0_range	34	th_knuckle_position
7	mf_proximal_length	21	ff_joint_3_range	35	ff_knuckle_position
8	mf_middle_length	22	ff_joint_2_range	36	mf_knuckle_position
9	mf_distal_length	23	ff_joint_1_range	37	rf_knuckle_position
10	rf_proximal_length	24	ff_joint_0_range	38	lf_knuckle_position
11	rf_middle_length	25	rf_joint_3_range	39	palm_shape
12	rf_distal_length	26	rf_joint_2_range	40	wrist_joints
13	lf_proximal_length	27	rf_joint_1_range	41	arm_length
14	lf_middle_length	28	rf_joint_0_range	42	elbow_joint_range

Table 4: **Space of robot parameter evolution for three-finger Jaco robot as target.** th, ff, mf, rt and lf represent thumb, first finger, middle finger, ring finger and little finger respectively. The robot evolution is described by $D = 42$ independent parameters in evolution in total.

C Learning Expert Dexterous Hand Robot Policy from Visual Human Demonstrations

Obtaining an expert policy on dexterous hand robot from human demonstration is the first step of our proposed pipeline. In Section 3.1 of the main paper, we provide a brief description of our approach. In this section, we provide more details on the technical approach of learning expert dexterous hand robot policy from *visual* human demonstration. It includes the reconstruction of simulation states from visual inputs using vision models, and learning through generated reverse curriculum from human demonstrations. We use DexYCB dataset [2] as an example to describe our method.

C.1 Simulation States from Visual Demonstration

Given the visual scene of human manipulation demonstration, the goal of this step is to reconstruct the simulation environment by recovering the underlying states from visual inputs so that the dexterous human robot can learn the same behavior as demonstrated by the human hand. The states include the 6D poses of the objects and the joint poses of the human hand.

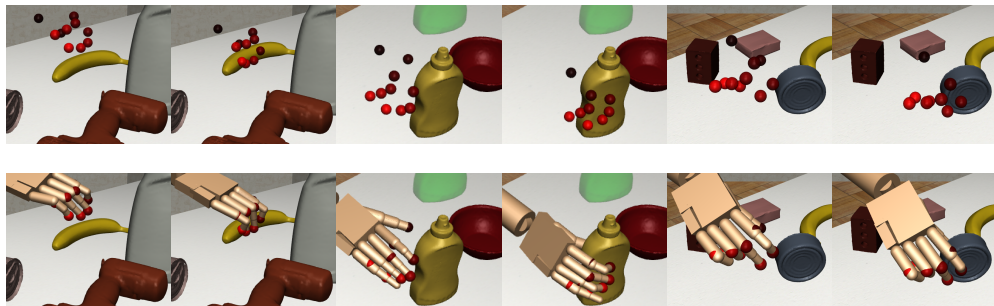


Figure 9: **Visualization of inverse kinematics (IK).** We use red spheres to show the hand 3D joint positions estimated by the vision model [63]. The second row is the result of using IK to fit the dexterous robot keypoints (i.e. finger tips and knuckles) to the corresponding human hand joint keypoints.

Object 6D Pose We use off-the-shelf models of CozyPose [64] to estimate the object 6D poses. CozyPose is a multi-view method for 6D object pose estimation. The object simulation states can be easily reconstructed by placing the scanned mesh model in the estimated 6D pose.

Dexterous Robot Pose We use off-the-shelf models of HRNet32 [63] to estimate the human hand joint poses. Due to the difference in shapes between the human hand and the dexterous robot, if we directly set the pose of the dexterous robot to be the estimated human hand pose, there could be an unwanted mismatch in the object grasping including penetration of object models, as pointed out by [16]. Therefore, we use inverse kinematics (IK) to minimize the average 3D distance between the positions of several dexterous robot joint keypoints and the corresponding human hand joint keypoints. We use ten joint keypoints, namely the tips and knuckles of the five fingers. To prevent the dexterous robot from penetrating the object mesh, we compute the volume of the intersection between the robot body mesh and the object mesh, and add the negative volume to the optimization objective of IK. We use the Powell algorithm [65] as the optimization algorithm for IK. We visualize several results of IK in Figure 9.

C.2 Curriculum for Learning Expert Policy on Dexterous Robot

Given the reconstructed simulation environment with the state-only trajectory estimated from vision models, our next goal is to train the expert policy on the dexterous hand robot to re-produce the same or similar behaviors as demonstrated by the human from visual input. Though recent literature [16, 66] have reported success on this problem, their implementations have not been released at the time of writing. We propose our solution to this task which is based on curriculum learning and reinforcement learning.

Our philosophy is to design a series of curricula to decompose the problem into multiple easier problems. Since we have access to the full state trajectory in DexYCB dataset demonstrations [2], we are able to reset the initial states of the simulation environment to the states at any timestamp in the demonstration trajectory.

During the first curriculum, the initial states of each simulation epoch are reset to be along the demonstrated trajectory while being very close to the set of goal states. With exploration, the agent can easily find trajectories of state-action pairs that lead to the goal. A policy can be trained with the explored trajectories. Then in the next curriculum, the initial states of each simulation epoch are still reset to be along the demonstration trajectory but move by a small distance in the reverse direction of demonstration compared to the first curriculum. During exploration, as long as the dexterous robot can enter the state regions explored and trained in the previous curriculum, it is easy for the trained policy to produce a state-action trajectory leading to the goal states. Then the policy is updated by training on the explored trajectories in the new curriculum. The above iteration of “initial state reverse movement + policy update” is repeated multiple times until reaching the desired initial state of the task. In this way, we will be able to decompose the difficult long-horizon continuous control tasks such as object manipulation into multiple easy tasks and finally solve the problem. The above learning process is illustrated in Figure 10.

Since we only use human demonstrations to reset epoch initial states, our curriculum strategy is able to deal with the task of one-shot learning from demonstration such as the case in the DexYCB

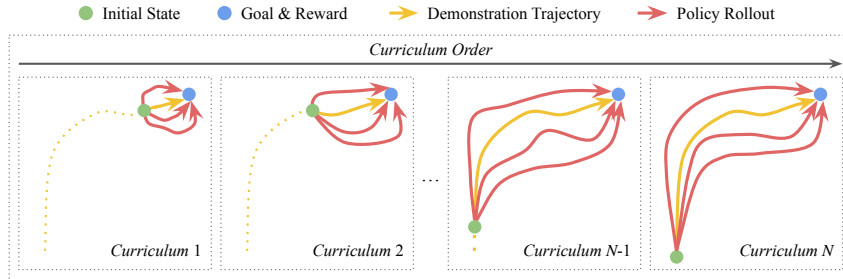


Figure 10: Curriculum learning of expert manipulation policy on dexterous hand robot.

dataset [2] where there is only one human demonstration video in each scene. We are also able to deal with noisy demonstrations such as the case of DexYCB dataset where the object and human states are estimated by vision models and could be noisy.

We point out that the similar idea of resetting simulation states for reverse curriculum generation can be found in previous work [67]. Different from [67], our curricula are generated along the human demonstration trajectory. Therefore, our curriculum design is more controllable and can train policies with behavior much closer to the human demonstration.

D Hyperparameter and Training Details

In this section, we present the hyperparameters and training procedures of our robot evolution and policy optimization. We use PyTorch [68] as our deep learning framework and NPG [61] as the RL algorithm in all experiments. To fairly compare against REvolveR [18], we use the same evolution progression step size ξ as [18] in the experiments. Since we use sparse reward setting in all experiments, in practice we use threshold in success rate q instead of episode reward in line 5 of Algorithm 1 of the main paper. The hyperparameters are illustrated in Table 5.

Hyperparameter	Value
RL Discount Factor γ	0.995
GAE	0.97
NPG Step Size	0.0001
Policy Network Hidden Layer Sizes	(32,32)
Value Network Hidden Layer Sizes	(32,32)
Simulation Epoch Trajectory Length	200
RL Training Batch Size	12
Evolution Progression Step Size ξ	0.03
Number of Sampled δ_i for Jacobian Estimation n	72
Evolution Direction Weight Factor λ	1.0
Sample Range Shrink Ratio λ_1	0.995
Success Rate Threshold q	0.667

Table 5: The value of hyperparameters used in our experiments.

E More Discussions

Evolution Path being Optimal? We point out that the proposed DEPS algorithm for joint optimization of robot evolution path and policy does not guarantee to find the optimal robot evolution path. In fact, finding such an optimal path is an NP-complete problem, similar to the ordinary path planning problem. However, we argue that our algorithm does provide a working solution that allows us to find an optimized and efficient robot evolution path for transferring the policy than naive linear evolution path, as shown by the reported experiment results.

Relation to Neural Architecture Search Our problem is closely related to the problem of Neural Architecture Search (NAS) [69, 70, 71] where we can view the intermediate robot in our problem as the neural network architecture in NAS. Similar to NAS where the goal is to optimize both network

architecture and network weights, the goal of our problem is also to optimize both the robot and the policy. However, our problem is different from NAS in that our problem is much noisier than NAS, where the converged neural network performance in NAS usually has a noise of 1-2% while the policy reward rollouts in our problem can have a noise up to 90% depending on the reward design. Therefore, solutions that use Bayesian Optimization for NAS such as [71] will not be able to work in our problem. In fact, our proposed DEPS algorithm is closer to differentiable neural architecture search [70].